J Mater Sci (2006) 41:5519–5525
DOI 10.1007/s10853-006-0307-1

# Effects of thickness and post deposition annealing on the properties of evaporated $In_2S_3$ thin films

**P. M. Ratheesh Kumar · Teny Theresa John · C. Sudha Kartha · K. P. Vijayakumar · T. Abe · Y. Kashiwaba**

Received: 29 August 2005 / Accepted: 20 October 2005 / Published online: 20 June 2006


**Abstract** Indium sulfide ($In_2S_3$) films with three different thicknesses (150, 400 and 600 nm) were prepared using thermal evaporation at room temperature. As prepared samples were amorphous and subsequent annealing at higher temperature (>573 K) resulted in the formation of crystalline phase. Optical band gap was found in the range of 1.9–2.9 eV for as prepared samples and decreased with increase in annealing temperature. Interference fringe like structure in transmission spectra revealed that the films were fairly smooth and reflective. Variations in electrical resistivity and photosensitivity as a function of film thickness and annealing temperature were studied. X-ray Photoelectron Spectroscopic (XPS) studies clearly indicated uniform distribution of both indium and sulphur along the film. Energy Dispersive X-ray analysis showed that as prepared samples were stoichiometric.

## Introduction

Indium sulfide ($In_2S_3$) is a compound, originating from II to VI structure, by replacing the divalent metal by a trivalent one. This generates a defect structure, in which sulfide forms a cubic or hexagonal close packed structure and part of the cation sites remain empty [1]. There are three forms of $In_2S_3$ viz., $\alpha$, $\beta$ and $\gamma$. Thin film of this semiconductor appears to be promising candidate for many applications in optoelectronic and photovoltaic devices. Photovoltaic junction is usually fabricated using CdS buffer layer in $CuInSe_2$, $CuInS_2$ and CdTe based solar cells [2, 3]. From an environmental point of view, the use of Cd should be avoided in CIS thin film solar cells. In addition, the band gap of CdS causes some optical absorption loss at short wavelengths. Therefore the research for a wider band gap semiconductor without CdS, has been performed by many research groups [3–5] recently. $In_2S_3$ can be used as an effective buffer layer in photovoltaic devices [6–8]. There are reports on the fabrication of photovoltaic junction by diffusing copper into CdS, so that first few layers of CdS get converted into p-type and hence forming homojunction [9]. An interesting point is that, if one could diffuse copper into $In_2S_3$, few layers of this may get converted into $CuInS_2$, which is a reasonably good absorber material for the solar cells and hence the fabrication of a photovoltaic junction could easily be realized. Recently we reported the fabrication of $CuInS_2/In_2S_3$ solar cells with a record efficiency of 9.5% using Chemical Spray Pyrolysis (CSP) technique [10].

A number of techniques have been used to prepare thin films of this compound such as Chemical Vapor Deposition [11], thermal evaporation [12], Chemical Spray Pyrolysis [3, 13] and rf sputtering [14].

However, there are only few reports of studies on vacuum deposited indium sulfide films and their characterization [12, 15, 16]. In most of these reports, $In_2S_3$ films were prepared by evaporating constituents elements, followed by the annealing. In this paper, we present a study of evaporated indium sulfide ($In_2S_3$) thin films prepared by

P. M. R. Kumar · T. T. John · C. S. Kartha · K. P. Vijayakumar (✉)
Thin Film Photovoltaic Division, Department of Physics, Cochin University of Science and Technology, Kochi 682022, India
e-mail: kpv@cusat.ac.in

T. Abe · Y. Kashiwaba
Department of Electrical and Electronic Engineering, Iwate University, Morioka 020 8551, Japan

directly evaporating the compound, which may be suitable for use as window layer in thin film solar cell devices. We were able to deposit stoichiometric films using this technique and optimized the experimental conditions, to make the film, suitable for using it as buffer layer in solar cell.

## Experimental procedure

Thin films of $In_2S_3$ having different thicknesses were prepared using vacuum evaporation technique. Cleaned micro glass slides with dimensions $40 \times 25 \times 1.4$ mm$^3$, were used as substrate. Vacuum chamber was pumped to $2 \times 10^{-7}$ Torr pressure before $In_2S_3$ evaporation and it was kept ~$10^{-6}$ Torr during the evaporation. Deposition was done keeping the substrate at room temperature. Material used for evaporation was $In_2S_3$ powder (Aldrich 99.999% purity). Rate of evaporation was kept constant at 2 nm/s. Deposition rate and thickness was monitored using quartz crystal oscillator. The thicknesses of the $In_2S_3$ samples were 150 (IS150), 400 (IS400) and 600 (IS600) nm. These were annealed in vacuum (at $2 \times 10^{-5}$ Torr) at four different annealing temperatures for 1 h. Heating and cooling rates were fixed at 2.5 K/min.

Structural properties of as prepared and annealed samples were determined using X-ray Diffraction (XRD) techniques employing Rigaku (D.Max.C) diffractometer having $CuK_\alpha$ radiation with $\lambda = 1.5405$ Å. XPS studies were performed with the help of ULVAC-PHI unit Model: ESCA 5600 CIM, capable of using argon ion sputtering for depth profiling. Optical properties were studied using optical absorbance and transmittance spectrum (UV VIS NIR spectrophotometer-Hitachi U-3410 model). Photosensitivity of the samples was measured as $S = (I_L - I_D)/I_D$ where $I_L$ is the current with illumination on and $I_D$ is the dark current of the sample [3, 17]. Photosensitivity and resistivity measurements were performed using Keithley 236 Source Measure Unit. Electrical contacts were given through two silver paint patches with a distance of 5 mm between them. For photosensitivity measurements, sample was illuminated using tungsten halogen lamp of power 100 mW/cm$^2$. Chemical composition of the films was analyzed using EDAX (Oxford systems, Model 6211). Fully quantitative results were obtained from the spectra by processing the data using ZAF correction program.

## Results and discussions

### Structural characterization

XRD analysis revealed that the as-prepared films were amorphous in nature, independent of film thickness. But annealing in vacuum resulted in crystallization of the samples. Figure 1 shows the XRD pattern of the samples annealed at 573 K. IS150 was amorphous at this temperature. IS400 was giving diffraction peaks corresponding to the tetragonal phases of $\beta$-$In_2S_3$ films only, but IS600 showed both $\beta$-$In_2S_3$ (tetragonal; JCPDS 25 390) and InS (cubic; JCPDS 19 588) phases with a preferential orientation along (109) plane. At 673 K, the sample IS150 was showing single orientation of $In_2S_3$ along (109) plane (Fig. 2). But still amorphous phase was more predominant. However, both IS400 and IS600 films consisted of multiple phases, when annealed at 673 K. Planes corresponding to tetragonal $\beta$-$In_2S_3$, cubic InS, and $In_6S_7$ (JCPDS 19 587) phases were observed in IS400 whereas, only tetragonal $\beta$-$In_2S_3$ and cubic InS phases appeared in IS600 with a preferential orientation along (103) plane.

Average crystallite size was calculated using Debye–Scherrer formula and found that grain size increased with increase in thickness and annealing temperature (Table 1). The result was attributed to relaxation of misfit strain with the formation of misfit dislocation in the films [18]. As the film thickness increased misfit strain decreased resulting in better crystallinity. Micro-cracks were not observed in the film, even after annealing at higher temperature, which was confirmed by SEM micrographs (Fig. 3).

### XPS studies

XPS analysis showed that indium and sulphur were uniformly distributed throughout the layer of both as prepared and annealed samples. Binding Energies (BE) of indium

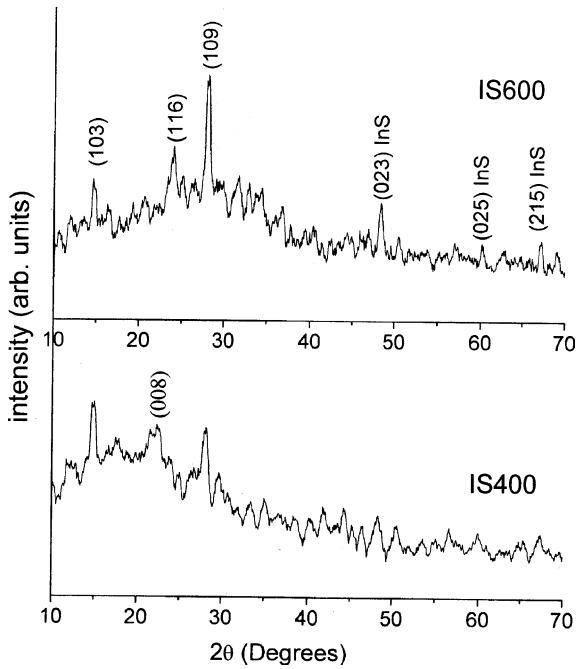


**Fig. 1** X-ray diffraction pattern of indium sulfide films annealed at 573 K

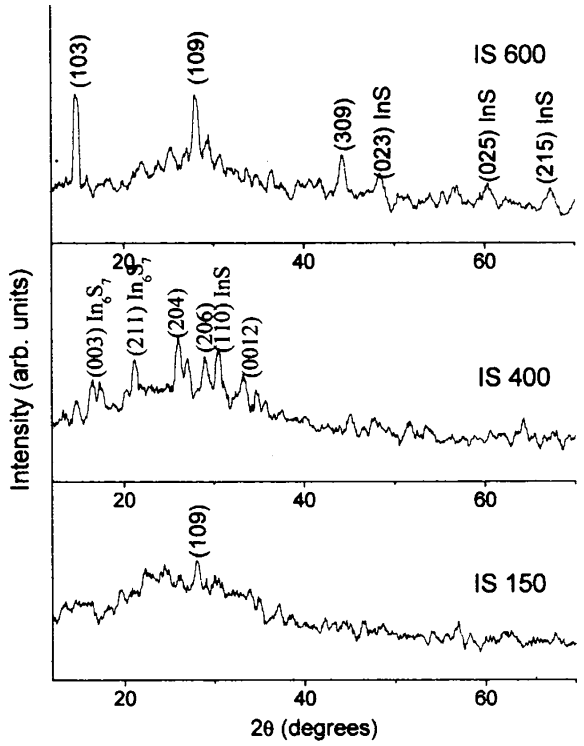


**Fig. 2** X-ray diffraction pattern $In_2S_3$ films at 673 K

(444.85 eV—In $3d_{5/2}$ and 452.85 eV—In $3d_{3/2}$) and sulphur (161.83 eV—S 2p) confirmed the formation of indium sulfide.

In IS150, a peak corresponding to a BE 174.58 eV for sulphur appeared and the exact chemical state of sulphur corresponding to this BE could not be identified (Fig. 4). When annealed at 673 K, this peak disappeared (Fig. 5). The peak height of sulphur in IS150 was small near the surface of the film in both annealed and as prepared samples. This was an indication of the oxygen substitution at sulphur position at the top surface of the film [3]. Oxygen was present in the film IS150 throughout the layer with a BE of 530.5 eV, which corresponded to that of $In_2O_3$. When annealed at 673 K, this peak disappeared. However, oxygen was present at the top of the surface with a BE of 533 eV in both as prepared and annealed samples, which was attributed to the surface contamination in the form of

**Table 1** Grain size variation with thickness and annealing temperature

| Sample thickness (nm) | FWHM (degrees) | | Grain size (Å) | |
|---|---|---|---|---|
| | 573 K | 673 K | 573 K | 673 K |
| 150 | Nil | 0.523 | Nil | 156.5 |
| 400 | 0.495 | 0.440 | 165.4 | 181.4 |
| 600 | 0.441 | 0.391 | 181.6 | 204.9 |

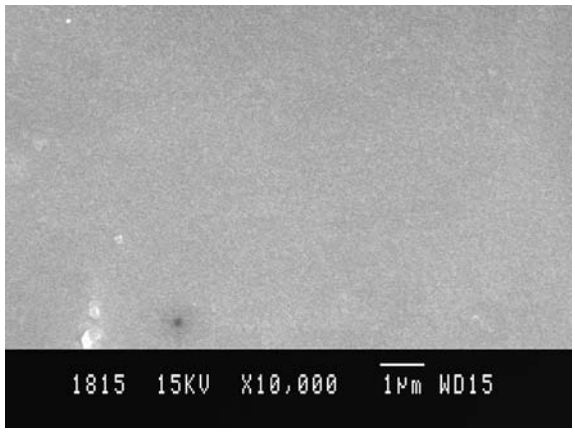


**Fig. 3** SEM image of sample IS600 annealed at 673 K

sulphate [3]. The appearance of a peak corresponding to the silicon was from the substrate.

Interestingly in IS600, no oxygen was present throughout the layer. However, a small shift in BE of indium and sulphur was seen at the top surface (Fig. 6), which was due to the presence of oxygen (535.75 eV) at the surface. But when annealed at 673 K, there was no shift in BE near the surface of the film and oxygen was present at the surface with a BE of 533 eV which corresponded to sulphate.

## EDAX analysis

Energy dispersive analysis of some of the as-prepared and annealed samples showed that, the stoichiometry and the composition of the film did not change much even after annealing. All the samples were slightly indium rich (In-44.34% and S-55.66%). But IS150 after annealing at 673 K, became indium deficient (In-36.19% and S-63.61%) while stoichiometry of IS600 remained the same even after the annealing at 673 K.

## Optical characterization

Optical characterization of both annealed and as-prepared samples of different thicknesses was done using optical absorption and transmission studies. Optical band gap was determined from the plot of $(\alpha h\nu)^2$ versus $h\nu$ graph by extrapolating the linear portion the curve to the $h\nu$ axis.

### *Effect of film thickness*

Absorption spectra (recorded in the wavelength range 400–900 nm) of samples with different thicknesses clearly indicated the shift of band gap towards lower values as thickness increased (Fig. 7). Band gap of the film IS150 was found to be equal to 2.85 eV. This large value of band gap was probably due to the presence of oxygen in the film [3]. Two band gaps were found in the samples IS400 and

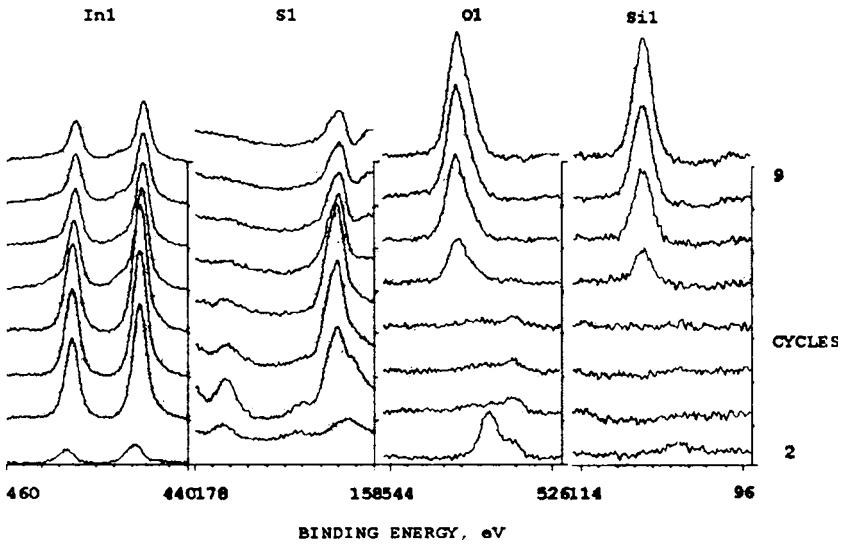


**Fig. 4** XPS depth profile of IS150

IS600. For IS400, values obtained were 1.88 eV and 2.4 eV while for IS600, these values were 2.0 eV and 2.22 eV. This might be due to the presence of InS phase along with $In_2S_3$ phase. Band gap of InS was reported to be 1.94 eV [15, 19]. This InS phase may be predominant in as prepared samples in amorphous state. Thickness dependence of band gap could arise due to one or combined effect of the following cause [20] (i) a large density of dislocations, (ii) quantum size effect and (iii) the change in barrier height due to change in grain size in polycrystalline films. Quantum size effect could be neglected due to the large film thickness [20]. Since, the as-prepared samples were amorphous in nature, grain size dependence on band gap also could also be omitted. Hence we suggest that band gap variation of the films with film thickness might be due to dislocations present in the films. Dislocations may reduce with the increase in film thickness.

Optical transmittance spectra of all the samples were recorded in the region 400–1500 nm (Fig. 8). Transmittance spectrum of the samples IS400 and IS600 exhibited interference fringe pattern, which revealed that film surface was fairly homogeneous and highly reflecting and there was not much scattering or absorption loss in the films. Almost flat transmittance spectrum was observed for IS150, since this thickness was too small to form interference fringes. It was also observed that, as the film thickness increased, the number of maximal and minimal extremes increased.

Film thickness and refractive index could be calculated using the envelope method, developed by Swanepol from transmission spectra, which is described elsewhere in detail [21]. Calculated thickness values were in very good agreement with the measured value. For IS400 thickness obtained was 373 nm while for IS600 this value was 617 nm. Refractive index of samples IS400 and IS600 was

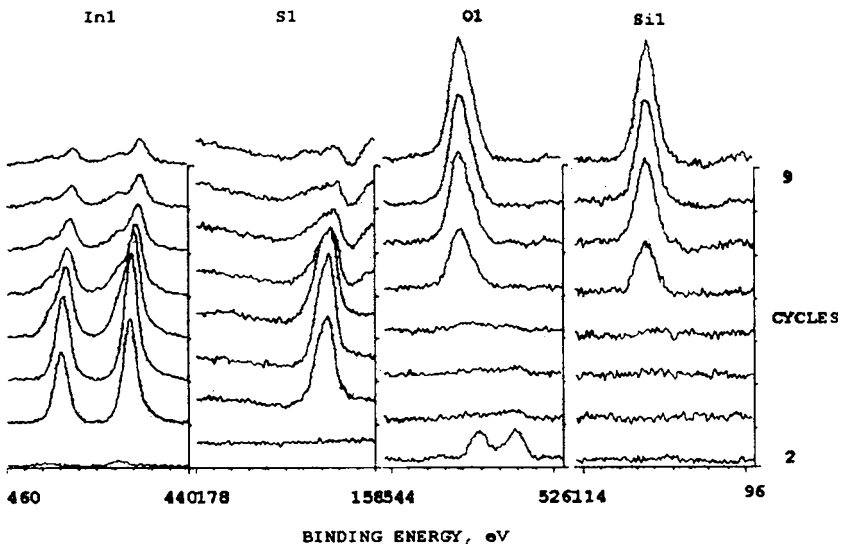


**Fig. 5** XPS depth profile of IS150 annealed at 673 K

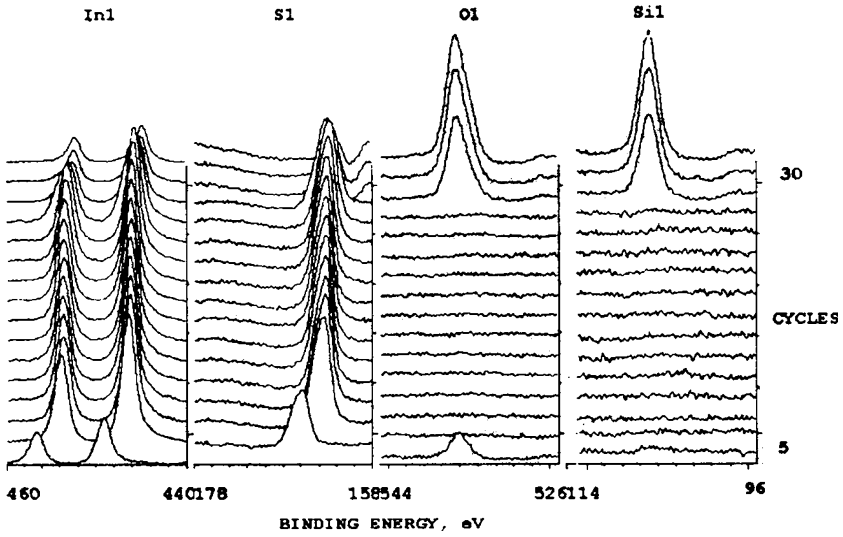


**Fig. 6** XPS depth profile of IS600

calculated and values were found in the range of 1.9–2.55. Since the transmission spectrum of the sample IS150 was flat, we could not use this for refractive index calculation.

*Effect of annealing temperature*

Band gap variation of all the samples is given in Fig. 9. For IS150, it decreased initially and then increased with annealing temperature. The increase in the band gap at higher annealing temperature might be due to the excess sulphur present in the film [3]. EDAX measurements also supported this argument. For the samples IS400 and IS600, band gap decreased with increase in the annealing temperature and this might be due to the better crystallinity of the film after annealing.

Interestingly, we were able to vary the band gap of $In_2S_3$ from 2.9 eV to 1.95 eV by varying either thickness or annealing temperature. The band gap obtained (2.94 eV) for the sample IS150, annealed at 673 K, was also having significance in solar cells applications as buffer layer. Wider band gap materials improve the light transmission in blue region resulting in increase of the short circuit current and open circuit voltage in solar cells.

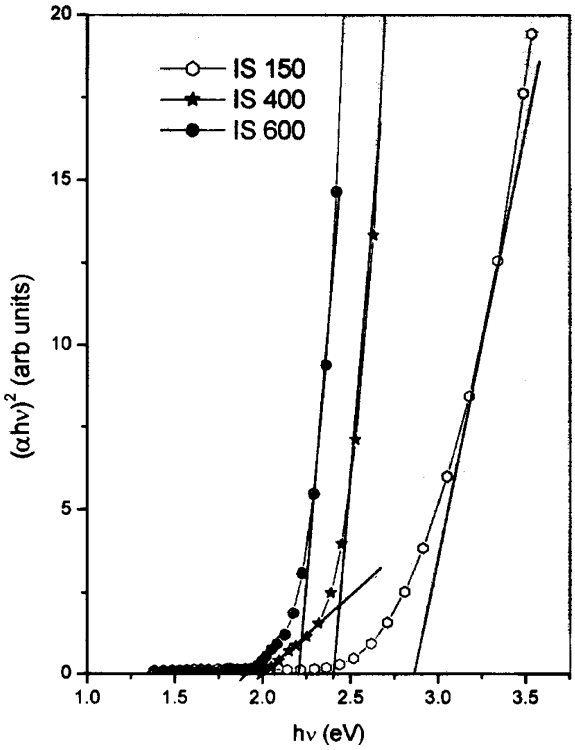


**Fig. 7** $(\alpha h\nu)^2$ versus $h\nu$ plot of $In_2S_3$ films of different thickness

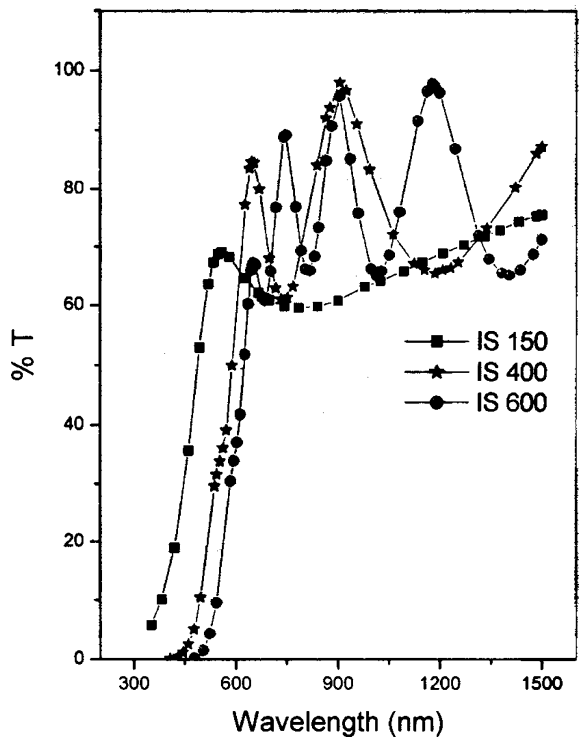


**Fig. 8** Transmission spectra of $In_2S_3$ films of different thickness

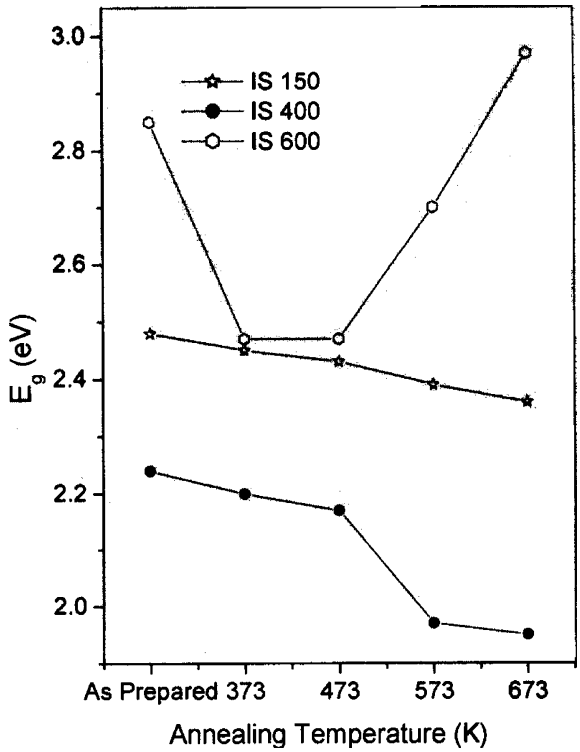


**Fig. 9** Variation in band gap of indium sulfide thin films with thickness and annealing temperature

Percentage of transmission decreased slightly with the increase in the annealing temperature for the sample IS400 and IS600. But for IS150, percentage of transmission increased at higher annealing temperature.

Electrical characterization

Electrical resistivity and photosensitivity measurements were done in all samples using two-probe method. Silver paste was painted uniformly over the sample for electrical contact.

*Effect of film thickness*

Dark electrical resistivity of all samples was measured and given in Table 2. Films were highly resistive (of the order of $10^4$ ohm cm) even though the samples were indium rich.

**Table 2** Variation of resistivity with annealing temperature

| Annealing temperature (K) | Resistivity (ohm cm) | | |
|---|---|---|---|
| | 150 nm | 400 nm | 600 nm |
| As prepared | $7.89 \times 10^4$ | $7.22 \times 10^4$ | $4.93 \times 10^4$ |
| 373 | $7.14 \times 10^4$ | $5.66 \times 10^4$ | $4.23 \times 10^4$ |
| 473 | $6.25 \times 10^4$ | $2.26 \times 10^4$ | $3.03 \times 10^3$ |
| 573 | $4.40 \times 10^4$ | $2.03 \times 10^4$ | $1.93 \times 10^3$ |
| 673 | $1.11 \times 10^4$ | $9.39 \times 10^3$ | $8.22 \times 10^2$ |

There was a slight decrease in resistivity with increase in film thickness. This behavior can be attributed to lattice defect such as vacancies, interstitials and dislocations, which might be formed through the first stage of the film growth. These defects might have added extra percentage to resistivity for thinner samples. The decrease in resistivity with increasing film thickness may be also attributed to the increase of the size of the individual crystallites. Photosensitivity increased with the increase in thickness for pristine samples (Table 3). Generally we expect a decrease in photosensitivity with decrease in resistivity, due to the increase in majority carrier concentration. But as the thickness increased, more absorption might be taking place resulting in larger number of minority carriers leading to photosensitivity for thicker samples.

*Effect of annealing temperature*

Resistivity and photosensitivity were decreasing with increase in annealing temperature for samples IS400 and IS600. But on increasing the annealing temperature, IS150 has lower resistivity and higher photosensitivity. From EDAX analysis of IS150, it was found that the sample became indium deficient on annealing. But still it was showing a decrease in the resistivity. Structural ordering of the film and also the increase in the grain size might be competing with the indium deficiency leading to reduction in resistivity. At higher annealing temperature, the sample had higher sulphur concentration, resulting in an increase of acceptors. This might be causing increase in minority carriers and hence leading to an increase in photosensitivity.

## Conclusion

Stoichiometric $\beta$-$In_2S_3$ films were prepared using thermal evaporation of the compound itself. As-prepared samples were amorphous, and crystallized at higher annealing temperature. Crystalline quality of the film was very much affected by the film thickness. Optical band gap decreased with the increase in film thickness. Electrical conductivity improved by post deposition annealing, but this may reduce photosensitivity for thicker samples. From the present

**Table 3** Variation of photosensitivity with annealing temperature

| Annealing temperature (K) | Photosensitivity $(I_L - I_D)/I_D$ | | |
|---|---|---|---|
| | 150 nm | 400 nm | 600 nm |
| As prepared | 0.296 | 10.497 | 14.695 |
| 373 | 0.061 | 6.613 | 12.693 |
| 473 | 0.026 | 3.618 | 5.586 |
| 573 | 2.493 | 0.579 | 5.788 |
| 673 | 6.794 | 0.302 | 1.478 |

study, it was observed that the sample having 150 nm thickness had largest band gap (2.9 eV). Again this sample exhibited highest photosensitivity and electrical conductivity on annealing at 673 K. Hence it could be concluded that samples having thickness 150 nm was good candidate for buffer layer in solar cells. Interestingly buffer layers are usually very thin films.

**Acknowledgements** One of the authors (PMR) is grateful to Ministry of Non-conventional Energy Sources for providing research fellowship and authors are thankful to Nuclear Science Centre, New Delhi for providing experimental facility. Another author (KPV) is thankful to Cochin University of Science & Technology for granting sabbatical leave for conducting this study. The authors also would like to thank UGC for financial assistance through the DSA II scheme. Financial assistance from Department of Science and Technology, India through FIST programme also acknowledged.

## References

1. Becker RS, Zheng T, Elton J, Saeki M (1986) Sol Energy Mater 13:97
2. O'Brien P, Octway DJ, Walsh JR (1998) Thin Solid films 315:57
3. John TT, Bini S, Kashiwaba Y, Abe T, Yasuhiro Y, Kartha CS, Vijayakumar KP (2003) Semicond Sci Technol 18:491
4. John TT, Sudha Kartha C, Vijayakumar KP, Abe T, Kashiwaba Y (2004) In: Proceedings of the 12th International conference on Solid Films and Surfaces (ICSFS-12), Hamamatzu, Japan, 2004
5. Kim W-T, Kim C-D (1986) J Appl Phys 60(7):2631
6. Spiering S, Eicke A, Hariskos D, Powalla M, Naghavi N, Lincot D (2004) Thin Solid Films 451–452:562
7. Spiering S, Hariskos D, Powalla M, Naghavi N, Lincot D (2003) Thin Solid Films 431–432:359
8. John TT, Kartha CS, Vijayakumar KP, Kashiwaba Y, Abe T (2004) Proceedings of the International Conference on the Physics, Chemistry and Engineering of Solar Cells (SCELL-2004) Badajoz, Spain, 2004
9. Kashiwaba Y, Kanno I, Ikeda T (1992) Jpn J Appl Phys 31:1170
10. John TT, Mathew M, Kartha CS, Vijayakumar KP, Abe T, Kashiwaba Y (2005) Sol Energy Mater Sol Cells 89:27
11. Bayon R, Maffiotte C, Herrero J (1999) Thin Solid Films 353:100
12. Shazly AAE, Elhady A, Metwally HS, Seyam MAM (1998) J Phys Condens Mater 10:5943
13. Bhira L, Essaidi H, Belgacem S, Couturier G, Salardenne J, Barreau N, Bernede JC (2000) Phys Stat Sol (a) 181:427
14. Ihara H, Abe H, Endo S, Irie T (1970) Solid State Commun 28:563
15. Seyam MAM (2001) Vacuum 63:441
16. Barreau N, Marsillac S, Bernède JC, Nasrallah TB, Belgacem S (2001) Phys Stat Sol (a) 184:179
17. Jiménez-Gonzaílez AE, Nair PK (1995) Semicond Sci Technol 10:1277
18. Myoung J-M, Yoon W-H, Lee D-H, Yun I, Bae S-H, Lee S-Y (2002) Jpn J Appl Phys 41:28
19. Takarabe K, Nishino T (1983) J Phys Chem Solids 44:681
20. Tyagi P, Vedeshwar AG (2001) Bull Mater Sci 24:297
21. Swanepoel R (1983) J Phys E: Sci Instrum 16:1214